J. Cent. South Univ. (2022) 29: 1274−1288
DOI: https://doi.org/10.1007/s11771-022-4999-4

Springer

Generalized plasticity model considering grain crushing and anisotropy for rockfill materials

ZHANG Xiang-tao(张向韬)[1], GAO Yi-zhao(高溢钊)[1], YU Yu-zhen(于玉贞)[1],
WANG Xiang-nan(王翔南)[1]*, ZHAN Zheng-gang(湛正刚)[2]

1. State Key Laboratory of Hydroscience and Engineering, Tsinghua University, Beijing 100084, China;
2. Power China Guiyang Engineering Co., Ltd., Guiyang 550081, China

Abstract: Rockfill materials have been widely used in the construction of rockfill dam, railway and highway subgrade due to its high filling density, good compaction performance, strong water permeability, small settlement deformation and high bearing capacity. A reasonable constitutive model for rockfill materials is very important for engineering computation and analysis, and has a great development space. Based on the crushing stress and spatial mobilized plane (SMP), a state parameter that can comprehensively reflect the anisotropy and grain crushing is proposed. This state parameter is used to improve the MPZ model (a modifed Zienkiewicz III model), so that a generalized plastic model is constructed to describe the stress and deformation characteristics of rockfill materials in engineering. The validity of the developed model is verified by a series of conventional triaxial tests with different inclination angles of the compaction plane. The variation trend of the constructed anisotropy index ω can reflect the non monotonic variation of the deformation and strength of rockfill with the direction angle of large principal stress, so the model can reflect the obvious difference caused by the initial anisotropy of rockfill on the mechanical properties.

Key words: constitutive model; anisotropy; grain crushing; rockfill materials

Cite this article as: ZHANG Xiang-tao, GAO Yi-zhao, YU Yu-zhen, WANG Xiang-nan, ZHAN Zheng-gang. Generalized plasticity model considering grain crushing and anisotropy for rockfill materials [J]. Journal of Central South University, 2022, 29(4): 1274−1288. DOI: https://doi.org/10.1007/s11771-022-4999-4.

1 Introduction

The deepening of human's understanding of natural phenomena is accompanied by the ever-increasing complexity and difficulty of scientific and engineering problems [1]. This raises higher requirements for methodologies that serve theoretical analysis and numerical simulation [2]. There is a definite need for developing advanced constitutive models to accurately simulate rockfill plastic deformation and failure in the fields of computational geosciences and engineering [3]. So it is necessary to comprehensively consider the engineering properties such as anisotropy and grain crushing.

Due to the large size of grains, it is difficult to carry out anisotropy tests of rockfill materials. However, through the tests of sands, we can know that the directional arrangement of grains has a significant impact on the anisotropic mechanical properties of granular materials [4 − 7]. When the

Foundation item: Project(2017YFC0404802) supported by the National Key R&D Program of China; Projects(U1965206, 51979143) supported by the National Natural Science Foundation of China; Project([2018]5630) supported by the Talents of Guizhou Science and Technology Cooperation Platform, China
Received date: 2021-05-18; **Accepted date:** 2021-10-08
Corresponding author: WANG Xiang-nan, PhD, Research Assistant; Tel: +86-13811583801; E-mail: 13684060651@163.com; ORCID: https://orcid.org/0000-0002-4470-681X

compaction plane of the specimen is inclined, the inclination angle δ will affect the stress − strain relationship of sands due to anisotropy. Specifically, some tests show that the peak strength of sands increases first and then decreases, rather than monotonically, with the increase of the inclination angle δ [8, 9]. In the anisotropic tests of rockfill materials, ZHANG et al [10] obtained similar characteristics as sands, but there are also differences: when the major principal strain ε_1 reaches 15%, the stress − strain curves of different inclination angles are still quite different; whereas in the ODA's tests of sands [9], the stress − strain curves tend to be consistent at ε_1=6%. This difference indicates that the constitutive model of sands can not be directly applied to rockfill materials.

Another important characteristic of rockfill materials is grain crushing, which has a significant influence on the strength, dilatancy and critical state of the rockfill materials. Many scholars have studied the grain crushing of rockfill materials. MARSAL [11] proposed a grain crushing index (B_g), which has been widely used in breakable soils (e.g., sand, road slag, and rockfill). XIAO et al [12] pointed out that grain crushing led to not only a vertical translation but also a rotation on the critical state line (CSL). LIU et al [13] within the framework of critical state, proposed two state functions that could reflect the dilatancy and strain softening of rockfill materials, revised the relative crushing index that proposed by HARDIN [14], and suggested an elastoplastic model that could describe grain crushing effect of the rockfill materials.

As for the constitutive model, the generalized plasticity model is a kind of elasto-plastic constitutive model, and it was first proposed by ZIENKIEWICZ et al [15]. PASTOR et al [16] subsequently developed the model into the Zienkiewicz III model (PZ model), which can reflect the main static and dynamic characteristics of geotechnical materials and has been widely applied [17 − 19]. Through introducing the critical state parameters into the PZ model, DONG [20] preliminarily modified the original model. The modified model (MPZ model) can better describe the nonlinear, dilatancy and strain hardening and softening characteristics of the stress − strain relationship of coarse grain materials, but cannot effectively reflect the influences of anisotropy and grain crushing.

At present, most of the models of rockfill materials are developed from the sand model, and these models are insufficient in the description of mechanical properties of rockfill materials. Therefore, it is necessary to establish a constitutive model that can comprehensively consider the anisotropy and grain crushing engineering properties of rockfill materials. In this study, an anisotropic state index is constructed according to the angle between spatial mobilized plane (SMP) and compaction plane. Considering the influence of grain crushing, an anisotropic compression line (ACL) is derived based on the crushing stress p_s with clear physical meaning. Combined with the anisotropic state index and ACL, a state parameter that can comprehensively consider grain crushing and anisotropy is proposed. In order to improve the stability and applicability of the constitutive model, the transformed stress method, the modified stress method, and a modified dilatancy equation are introduced [21 − 23]. Based on the above considerations, a generalized plastic model for rockfill materials (PZR model) is developed from the MPZ model. A series of conventional triaxial tests with different inclination angles are simulated to verify the applicability of the proposed model.

2 Original generalized plastic model (MPZ model)

The elastic volumetric strain and the elastic shear strain are respectively controlled by the volumetric modulus K_{ev} and the shear modulus G_{es}:

$$\Delta\varepsilon_v^e = \frac{\Delta p}{K_{ev}},\ \Delta\varepsilon_s^e = \frac{\Delta q}{3G_{es}} \tag{1}$$

where Δq is the increment of the generalized shear stress; Δp is the increment of the mean effective stress; $\Delta\varepsilon_v^e$ is the increment of the elastic strain; and $\Delta\varepsilon_s^e$ is the increment of the elastic shear strain.

The elastic modulus varies with changes of the mean effective stress p and the void ratio e [24]:

$$K_{ev} = K_0\frac{(2.97 - e)^2}{1 + e}p_a\left(\frac{p}{p_a}\right)^{1/2} \tag{2}$$

$$G_{es} = G_0\frac{(2.97 - e)^2}{1 + e}p_a\left(\frac{p}{p_a}\right)^{1/2} \tag{3}$$

where K_0 and G_0 are model constants; and p_a is the atmospheric pressure. Next, the plastic part of the model is introduced.

1) The critical state and corresponding parameters

The critical state refers to the state in which the mean effective stress p, the general shear stress q, and the void ratio remain unchanged, while the shear strain ε_d develops indefinitely when the soil is subjected to shear action that results in failure [25].

$$\dot{p} = \dot{q} = \dot{\varepsilon}_v = 0, \dot{\varepsilon}_d \neq 0 \tag{4}$$

where ε_v is the volumetric strain and the superscript "•" means the rate of change.

The soil under different drainage conditions and stress paths will reach a spatial curve as the following form [26], namely critical state line (CSL), when the soil reaches the critical state:

$$e_c = e_\Gamma - \lambda_c\left(\frac{p}{p_a}\right)^\zeta \tag{5}$$

where e_Γ, λ_c and ζ are constants. For sands, the value of ζ is about 0.7, while for rockfill materials, ζ has different values in different grain crushing cases.

The state parameter is defined by the following Eq. [27]:

$$\psi = e - e_c \tag{6}$$

where e is the current void ratio and e_c is the critical void ratio corresponding to the current mean effective stress.

2) Loading direction and plastic flow direction

Referring to the expression of LI et al [28], the state parameter ψ is introduced into the dilatancy equation:

$$d_g = \left(1 + \alpha_g\right)\left(M_d - \eta\right) \tag{7}$$

$$M_d = M_g\exp\left(m_g\psi\right) \tag{8}$$

where η=q/p, $\alpha_g$and m_g are model constants; and M_d is expressed as the phase transformation stress ratio, that is, the stress ratio corresponding to the transformation state from volumetric contraction to volumetric expansion; $M_g$corresponds to the slope of the projection of CSL on the p−q plane.

The plastic flow direction corresponding to dilatation is as follows:

$$\boldsymbol{n}_{gL} = \frac{1}{\sqrt{1 + d_g^2}}\left(d_g, 1\right)^T \tag{9}$$

When unloading, the plastic flow direction is specified as:

$$\boldsymbol{n}_{gU} = \frac{1}{\sqrt{1 + d_g^2}}\left(-d_g, 1\right)^T \tag{10}$$

The non-associated flow rule is adopted, so that the expression form of the unit loading direction vector $\boldsymbol{n}_f$ is similar to that of $\boldsymbol{n}_g$:

$$\boldsymbol{n}_f = \frac{1}{\sqrt{1 + d_f^2}}\left(d_f, 1\right)^T \tag{11}$$

$$d_f = \left(1 + \alpha_f\right)\left(M_f - \eta\right) \tag{12}$$

where α_f is a model constant. The $g(\theta)$ method is used to extend Eqs. (9)−(11) from the triaxial stress space to the three-dimensional stress space, and the expressions are:

$$\begin{cases} M_f = g\left(\theta, c\right)M_{fc} \\ M_g = g\left(\theta, c\right)M_{gc} \end{cases} \tag{13}$$

$$c = M_e/M_c \tag{14}$$

$$g\left(\theta, c\right) = \frac{2c}{\left(1 + c\right) - \left(1 - c\right)\sin 3\theta} \tag{15}$$

where M_{gc} and M_{fc} are M_g and M_f under triaxial compression, respectively; M_e and M_c are the peak stress ratios under triaxial extension and triaxial compression.

3) The plastic modulus

The plastic modulus of MPZ model is expressed as follows:

$$H_L = H_0 p' H_f H_v H_{DM} H_{den} \tag{16}$$

$$H_0 = H_{L0}\exp\left(-\beta_H\psi\right) \tag{17}$$

where H_0 refers to the improved benchmark plastic modulus considering stress state [29, 30], while β_H and H_{L0} are non-negative model constants.

H_f is used to describe the shear mapping rules, which can be expressed by the stress ratio η, as shown in Eq. (18). η_f is the stress ratio in the original point of the yield surface, as shown in Eq. (19).

$$H_f = (1 - \eta/\eta_f)^4 \tag{18}$$

$$\eta_f = (1 + 1/\alpha_f)M_f \tag{19}$$

H_v can describe the phenomenon of strain softening, which is related to the stress state:

$$H_{\mathrm{v}} = 1 - \frac{\eta}{M_{\mathrm{b}}} \tag{20}$$

$$M_{\mathrm{b}} = M_{\mathrm{g}}\exp\left(-m_{\mathrm{b}}\psi\right) \tag{21}$$

where m_{b} is a non-negative model constant. When the initial state of the soil material is relatively dense, $\psi<0$, and thus $M_{\mathrm{b}}>M_{\mathrm{g}}$. In this case, there will be the state of $\eta>M_{\mathrm{g}}$ and $H_{\mathrm{v}}>0$. After the state changes from volumetric contraction to volumetric expansion, ψ gradually approaches 0, leading to a reduction of M_{b}. Gradually, the peak intensity is reached, followed by the strain softening, which corresponds to a negative H_{v} with $\eta>M_{\mathrm{b}}$.

H_{DM} reflects the influence of the stress history on the plastic modulus, and H_{den} is used to represent the compaction and hardening effects of coarse soils. Their expressions are shown in Eqs. (22)−(24):

$$H_{\mathrm{DM}} = \left(\frac{\zeta_{\max}}{\zeta}\right)^{\gamma} \tag{22}$$

$$\zeta = p\left(1 - \frac{\eta}{\eta_{\mathrm{f}}}\right)^{-1/\alpha_{\mathrm{f}}} = p\left[1 - \left(\frac{\alpha_{\mathrm{f}}}{1+\alpha_{\mathrm{f}}}\right)\frac{\eta}{M_{\mathrm{f}}}\right]^{-1/\alpha_{\mathrm{f}}} \tag{23}$$

$$H_{\mathrm{den}} = \exp\left(r_{\mathrm{den}}\varepsilon_{\mathrm{v}}\right) \tag{24}$$

where γ and r_{den} are model constants. Moreover, the plastic unloading modulus is modified to consider the influence of the confining pressure:

$$H = \begin{cases} H_{\mathrm{U0}}H_{\mathrm{den}}p_{\mathrm{a}}\left(\dfrac{p}{p_{\mathrm{a}}}\right)^{1/2}\left(\dfrac{M_{\mathrm{g}}}{\eta_{\mathrm{U}}}\right)^{\gamma_{\mathrm{U}}}, & \dfrac{M_{\mathrm{g}}}{\eta_{\mathrm{U}}} > 1 \\ H_{\mathrm{U0}}H_{\mathrm{den}}p_{\mathrm{a}}\left(\dfrac{p}{p_{\mathrm{a}}}\right)^{1/2}, & \dfrac{M_{\mathrm{g}}}{\eta_{\mathrm{U}}} < 1 \end{cases} \tag{25}$$

where H_{U0} and γ_{U} are model constants; and η_{U} is the stress ratio corresponding to the stress reversal.

3 Developed generalized plasticity model for rockfill materials (PZR model)

The MPZ model introduced above does not consider the effects of anisotropy and grain crushing on the mechanical properties, which, however, are ubiquitous in the engineering and are thus very important for the evaluation of stress and deformation. In the following part, an anisotropic state parameter considering anisotropy and grain crushing is proposed to modify the MPZ model.

3.1 Yield surface

As mentioned above, the MPZ model does not need an explicit yield function. Nevertheless, if the yield function can be specifically expressed for the theoretical derivation, it can be used as a reference for further improvement in the theoretical analysis. The yield surface of the MPZ model can be obtained by integrating the loading direction vector as expressed in Eqs. (11) and (12) [31]:

$$f = q - M_{\mathrm{f}}p\left(\frac{1+\alpha_{\mathrm{f}}}{\alpha_{\mathrm{f}}}\right)\left[1 - \left(\frac{p'}{p_{\mathrm{x}}}\right)^{\alpha_{\mathrm{f}}}\right] \tag{26}$$

where p_{x} is the intersection point between the yield surface and the p-axis.

3.2 Description of anisotropic state of rockfill materials

The compaction plane is produced by the directional grain arrangement. Many experiments and mesoscopic mechanics analyses have shown that the direction of the long axis of grains can basically remain unchanged even in the case of large macroscopic shear deformation, but the size and shape of pores, the number and direction of contacts are greatly changed during shearing [32−34]. However, in practical engineering, the strain generated by the loading of the rockfill material generally does not exceed 2%, although it can reach 10% locally.

The inclination angle of compaction plane has a significant effect on the mechanical properties of the rockfill material. In order to reflect this effect in the constitutive model, it is necessary to properly describe the anisotropic fabric and define the anisotropic state index.

1) Description of the anisotropic fabric

Based on the above analysis, the transversely isotropic fabric tensor is introduced as [22]:

$$\boldsymbol{F}_{ij} = \begin{pmatrix} \dfrac{(1+\Delta)+(3\Delta-1)\cos 2\delta}{4} & 0 & \dfrac{(3\Delta-1)\sin 2\delta}{4} \\ 0 & \dfrac{1-\Delta}{2} & 0 \\ \dfrac{(3\Delta-1)\sin 2\delta}{4} & 0 & \dfrac{(1+\Delta)+(1-3\Delta)\cos 2\delta}{4} \end{pmatrix} \tag{27}$$

where Δ is the concentration index that measures the grain's long axis, and δ is the degree rotated around

the x-axis by the compaction plane (the arrangement direction of the long axis).

The concept of the modified stress is expressed as follows [22]:

$$\bar{\sigma}_{ij} = \frac{3}{2}\left(\sigma_{ik}F_{kj} + F_{ik}\sigma_{kj}\right) \tag{28}$$

where $\bar{\sigma}_{ij}$ is the modified stress tensor, and σ_{ij} is the real stress tensor. After such treatment, the modified stress tensor applied in the direction perpendicular to the long axis of grains is smaller than the real stress tensor, which is equivalent to the modulus increasing in this direction. This method can help effectively calculate the lateral strain inconsistency caused by the fabric anisotropy, which is an advantage over many other anisotropic methods such as the joint invariant method and the loading angle method.

2) The anisotropic state index

The tests of rockfill materials show that the strength of specimens decreases as the inclination angle δ increases from 0° to 75°, whereas increases when δ aproches 90° [10]. However, the modified stress method fails to reflect the non-monotonic variation of the peak anisotropy intensity. Therefore, the concept of spatially mobilized plane (SMP; Figure 1) is introduced into the model [35]. The SMP has a clear physical significance that the ratio of the shear stress τ_{SMP} to the normal stress σ_{SMP} is the largest on the corresponding SMP. Thus, the grains on SMP are most likely to slide. Moreover, the SMP changes simultaneously as the loading path varies, which affects the apparent strength of specimens. Theoretically, when SMP and the compaction plane coincide, the strength of the soil is the lowest.

For the soil element, there are four pairs of SMPs in the principal stress space, and each pair of SMPs is parallel to each other. The minimum angle $\alpha_{\min}$ between SMP and the compaction plane is expressed as follows:

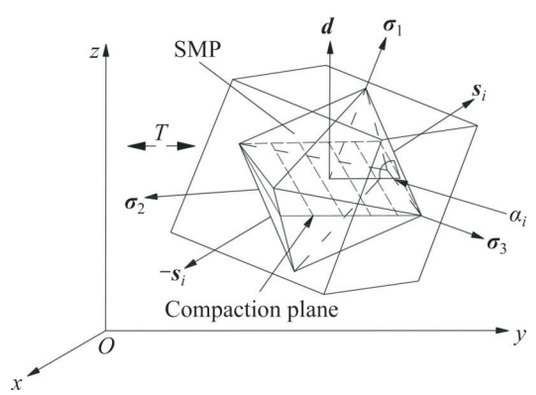

Figure 1 Schematic diagram of angle between SMP and compaction plane

$$\alpha_{\min} = \min\left(\alpha_1, \alpha_2, \alpha_3, \alpha_4\right) \tag{29}$$

where α_i (i=1, 2, 3, 4) is the angle between the four pairs of SMPs and the compaction plane, as shown in Figure 1, and the expression of cosα_i is:

$$\cos\alpha_i = \cos\left(\boldsymbol{t}_i, \boldsymbol{d}\right) = \frac{\left|t_{i1}d_z + t_{i2}d_x + t_{i3}d_y\right|}{\sqrt{t_{i1}^2 + t_{i2}^2 + t_{i3}^2}\sqrt{d_z^2 + d_x^2 + d_y^2}} \tag{30}$$

$$\boldsymbol{t}_i = \boldsymbol{T}\boldsymbol{s}_i \tag{31}$$

$$\boldsymbol{d} = \left(d_z, d_x, d_y\right)^{\mathrm{T}} \tag{32}$$

where d_x, d_y and d_z are respectively the cosine values of the angles between the normal vector of the compaction plane and the basis vector of the physical space; $\boldsymbol{t}_i$ is the normal vector of the four groups of SMPs in the physical space; and $\boldsymbol{T}$ is the transformation matrix from the stress space to the physical space:

$$\boldsymbol{T} = \begin{bmatrix} l_1 & l_2 & l_3 \\ m_1 & m_2 & m_3 \\ n_1 & n_2 & n_3 \end{bmatrix} \tag{33}$$

where l_i, m_i, n_i (i=1, 2, 3) are the cosines of the principal stress σ_i relative to the three directions of the basis vectors of the physical space.

The normal vectors of four pairs of SMPs are denoted as $\boldsymbol{s}_1$, $\boldsymbol{s}_2$, $\boldsymbol{s}_3$ and $\boldsymbol{s}_4$, respectively.

$$\begin{cases} \boldsymbol{s}_1 = \left(a_1, a_2, a_3\right) \\ \boldsymbol{s}_2 = \left(a_1, -a_2, -a_3\right) \\ \boldsymbol{s}_3 = \left(a_1, -a_2, a_3\right) \\ \boldsymbol{s}_4 = \left(a_1, a_2, -a_3\right) \end{cases} \tag{34}$$

where a_1, a_2 and a_3 are directional cosines of SMP in the principal stress space, respectively:

$$a_1 = \sqrt{\frac{I_3}{\sigma_1 I_2}},\ a_2 = \sqrt{\frac{I_3}{\sigma_2 I_2}},\ a_3 = \sqrt{\frac{I_3}{\sigma_3 I_2}} \tag{35}$$

where I_1, I_2 and I_3 are the first, second, and third principal invariants, respectively:

$$\begin{cases} I_1 = \sigma_{ii} \\ I_2 = \dfrac{1}{2}\left[\left(\sigma_{ii}\right)^2 - \sigma_{\mathrm{rs}}\sigma_{\mathrm{sr}}\right] \\ I_3 = \dfrac{1}{3}\sigma_{ij}\sigma_{jk}\sigma_{ki} - \dfrac{1}{2}\sigma_{\mathrm{rs}}\sigma_{\mathrm{sr}}\sigma_{mn} + \dfrac{1}{6}\left(\sigma_{nn}\right)^3 \end{cases} \tag{36}$$

The $\alpha_{\min}$ calculated from Eqs. (29) and (30) is a scalar varying with the development of stress, which has a clear physical meaning and can reflect the degree of mutual deviation between SMP and the compaction plane in real time. When SMP is parallel to the compaction plane, $\alpha_{\min}$=0, and the soil is most prone to shear deformation.

Therefore, considering the changes in state parameters caused by the long-axis orientation of grains, $\alpha_{\min}$ can be introduced to construct a new form of the anisotropic state index ω:

$$\omega = \left(\sin\alpha_{\min}\right)^r \tag{37}$$

where r is a model constant, which can effectively reflect the differentiation degree of the anisotropic states caused by the change of $\alpha_{\min}$.

Figure 2 shows the variation of $\alpha_{\min}$ with δ in conventional triaxial compression tests. As the loading process advances, the SMP deflects with the change of stress state, and finally a relatively stable value is reached. When the strain is large, δ =0° corresponds to the maximum $\alpha_{\min}$, while δ=60° and δ =75° correspond to the minimum $\alpha_{\min}$, which can reflect the non-monotonic variation trend of the specimen strength with δ.

Equation (37) is introduced into the original state parameter ψ to form a new parameter considering the anisotropic state:

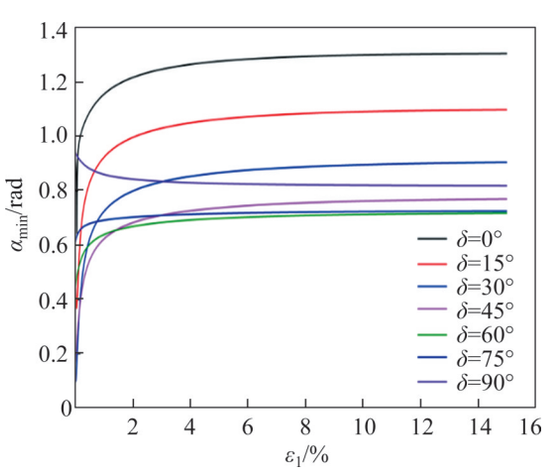

Figure 2 Variation of $\alpha_{\min}$ with δ in conventional triaxial compression tests

$$\xi = \psi - \Gamma\omega \tag{38}$$

where Γ is a model constant, which can reflect the influence of the real-time anisotropy represented by $\alpha_{\min}$ on the position of the reference state line.

In summary, the modified stress method is able to calculate the true strain value of each direction under the three-dimensional stress state, while the anisotropic state index ω is favored by its capacity to reflect the non-monotonic variation of the peak intensity of the anisotropy as δ varies, which is not possible for the modified stress method.

3.3 Anisotropic compression line considering grain crushing

In the MPZ model, only the CSL in the form of a curve projected on the $e-\ln p$ plane is given, no correlation quantity can reflect the grain crushing, which makes the model have certain arbitrariness in reflecting grain crushing. The research shows that the contribution of the plastic work done by p and q to the grain crushing of rockfill materials differs as the stress state varies. Consequently, using the conventional triaxial test to simulate the grain crushing under the complex stress path has a large error [36]. Given the limited ability of the constitutive model to accurately calculate the plastic strain increment under various complex stress paths, it is not accurate to use the relationship between the plastic work and the relative crushing rate to reflect the impact of the rockfill grain crushing on mechanical properties. In this study, the contribution of work done by p and q to grain crushing is considered respectively by the crushing stress p_s and the offset of ACL caused by shear [37, 38].

1) The normal compression line

The normal consolidation line (NCL) of the Cambridge model and the modified Cambridge model is straight in the $e-\ln p$ plane:

$$e = N - \lambda\ln p \tag{39}$$

where N is the void ratio when the mean stress p on the NCL is 1 kPa; λ is the slope of the NCL in the $e-\ln p$ plane.

Equation (39) is mainly applicable to normally consolidated clay and light overconsolidated clay. For cohesionless granular materials such as rockfill, the NCL under different initial densities is different and shows obvious nonlinearity. Under high

confining pressure, the NCLs converge to an asymptote due to grain crushing [39]. In the process of isotropic compression, the volumetric deformation under low confining pressure mainly comes from the elastic change of soil skeleton and the sliding and rotation of grains; under high confining pressure, due to grain crushing of soil, the deformation will increase significantly [39]. Moreover, some scholars have drawn similar conclusions by using the micro-macro volume averaging approach in the framework of themomechanics [40]. In this study, the crushing stress p_s corresponds to the point of maximum curvature of the NCL in the $e-\ln p$ plane. When p is greater than the representative crushing stress, the amount of grain crushing of the rockfill material will increase significantly. At this point, the compression deformation rate of the rockfill volume is the largest, and eventually it converges to an asymptote, which is equivalent to NCL in the normally consolidated clay, and can be expressed as follows:

$$e = Z - \lambda \ln\left(\frac{p + p_s}{1 + p_s}\right) \tag{40}$$

$$p_s = \exp\left(\frac{N - Z}{\lambda}\right) - 1 \tag{41}$$

where Z is the void ratio of rockfill on the NCL when p equals 1 kPa, which determines the starting position of NCL; λ is the slope of the NCL in the $e-\ln(p+p_s)$ space (Figure 3).

2) The anisotropic compression line

As shown in Figure 3, the elastic line of the rockfill material is expressed as:

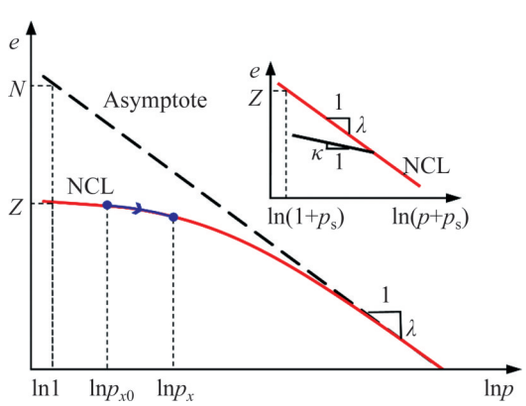

Figure 3 NCL considering grain crushing in $e-\ln p$ space and $e-\ln(p+p_s)$ space [39]

$$e = e_0 - \kappa \ln\left(\frac{p + p_s}{p_0 + p_s}\right) \tag{42}$$

where κ is the slope of the rebound line in the $\ln(p+p_s)$ space. When a soil specimen is compressed from p_{x0} to p_x, according to Eq. (40), the total volumetric strain in the loading process can be deduced as:

$$\varepsilon_v = \frac{\lambda}{1 + e_0} \ln\left(\frac{p_x + p_s}{p_{x0} + p_s}\right) \tag{43}$$

According to Eq. (42), the elastic volumetric strain can be expressed as:

$$\varepsilon_v^e = \frac{\kappa}{1 + e_0} \ln\left(\frac{p_x + p_s}{p_{x0} + p_s}\right) \tag{44}$$

According to Eqs. (43) and (44), the plastic volumetric strain can be expressed as:

$$\varepsilon_v^p = \frac{\lambda - \kappa}{1 + e_0} \ln\left(\frac{p_x + p_s}{p_{x0} + p_s}\right) \tag{45}$$

According to Eq. (45), the expression of p_x in the loading process can be obtained:

$$p_x = \left(p_{x0} + p_s\right) \exp\left(\frac{\varepsilon_v^p}{c_p}\right) - p_s \tag{46}$$

By substituting Eq. (46) into Eq. (26), the yield function can be expressed as:

$$f = q - M_f p \left(\frac{1 + \alpha_f}{\alpha_f}\right) \cdot \left[1 - \left(\frac{p}{\left(p_{x0} + p_s\right) \exp\left(\frac{\varepsilon_v^p}{c_p}\right) - p_s}\right)^{\alpha_f}\right] \tag{47}$$

To enable reference line to quantitatively reflect the different state parameters caused by grain crushing under different shear effects, the concept of the anisotropic compression line (ACL) is introduced [38]. Specifically, as η increases from 0 to M, the ACL moves from NCL to CSL (Figure 4).

Figure 4 shows the NCL, ACL, CSL and the state parameter in the $e-\ln p$ space. From point D to point E along the mean stress path (Figure 4), it can be concluded according to the yield function Eq. (47) that the change of the void ratio caused by the shear stress in the loading process is:

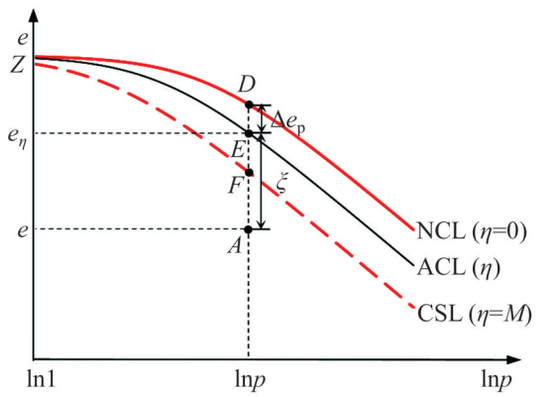

Figure 4 NCL, ACL, CSL, and state parameter ξ of granular soil in $e-\ln p$ space [38]

$$\Delta e_{\mathrm{p}}=(\lambda-\kappa)\ln\left[\frac{\left(1-\dfrac{\alpha_{\mathrm{f}}\eta}{M_{\mathrm{f}}(1+\alpha_{\mathrm{f}})}\right)^{-\frac{1}{\alpha_{\mathrm{f}}}}p+p_{\mathrm{s}}}{p+p_{\mathrm{s}}}\right] \tag{48}$$

According to Eq. (40), the void ratio of point D can be calculated. Combined with the variation of the void ratio of point E loaded by the mean stress path, the void ratio e_η of point E can be obtained as shown in Eq. (49).

$$e_\eta=Z-\lambda\ln\left(\frac{p+p_{\mathrm{s}}}{1+p_{\mathrm{s}}}\right)-(\lambda-\kappa)\ln\left[\frac{\left(1-\dfrac{\alpha_{\mathrm{f}}\eta}{M_{\mathrm{f}}(1+\alpha_{\mathrm{f}})}\right)^{-\frac{1}{\alpha_{\mathrm{f}}}}p+p_{\mathrm{s}}}{p+p_{\mathrm{s}}}\right] \tag{49}$$

3.4 State parameter considering anisotropy and grain crushing

By substituting Eq. (49) into Eq. (6) and introducing ψ into Eq. (38), the state parameter considering the anisotropic state and grain crushing is obtained:

$$\xi=e-e_\eta-\Gamma\omega \tag{50}$$

where $e_\eta+\Gamma\omega$ can be regarded as the reference state line. The above equation can not only reflect the effect of grain crushing on the reference line, but also consider the effect of the real-time anisotropy represented by the SMP on the position of the reference line. This is the core of constructing a new constitutive model for the rockfill. The new state parameter varying with load is used to replace the state parameter calculated by the fixed CSL of the original model. Therefore, the main characteristics of the stress deformation of the rockfill material can be reflected in theory.

3.5 Modification of dilatancy equation

The dilatancy equation is an important part of the constitutive model, and has a great influence on the prediction of volumetric strain. It can be linear or nonlinear, and the most well-known ones are probable the Nova's equation [41].

$$d_{\mathrm{g}}=(1+\alpha_{\mathrm{g}})(M-\eta) \tag{51}$$

and the equation of the modified Cam-clay model [42], separately:

$$d_{\mathrm{g}}=\frac{M^2-\eta^2}{2\eta} \tag{52}$$

where α_{g} is a constant and M is the phase transformation stress ratio. Nova's equation is the original form of Eq. (7). However, both of them are limited in simulating the dilatancy behavior of rockfill materials. On the one hand, the plastic shear strain should theoretically be 0 in the case of isotropic compression. So there is a mismatch in the linear dilatancy equation at the point of isotropic compression. On the other hand, the equation of the modified Cam-clay model overestimates the dilatancy of rockfill under low confining pressure [43]. Based on the above considerations, the PZR model adopts a dilatancy equation considering the stress–strain characteristics of typical granular materials and the changes of mesoscopic structures [23]:

$$\frac{\mathrm{d}\varepsilon_{\mathrm{v}}^{\mathrm{p}}}{\mathrm{d}\varepsilon_{\mathrm{d}}^{\mathrm{p}}}=\frac{mM^{m+1}-m\eta^{m+1}}{(m+1)\eta^m} \tag{53}$$

where M is the phase transformation stress ratio and m is a model constant. When m equals 1, the above equation degenerates to the dilatancy equation of the modified Cambridge model. Meanwhile, when $\eta=M$, the first-order Taylor expansion of Eq. (53) will be identical to the dilatancy equation used in the original MPZ model.

Considering that the dilatancy of the rockfill material is significantly affected by anisotropy, the anisotropic state parameter ξ proposed in this study is introduced into Eq. (53) :

$$d_g = \frac{\mathrm{d}\varepsilon_v^p}{\mathrm{d}\varepsilon_d^p} = \frac{mM_d^{m+1} - m\eta^{m+1}}{(m+1)\eta^m} \tag{54}$$

$$M_d = M_c \exp\left(m_g \xi\right) \tag{55}$$

where M_d is the phase transformation stress ratio related to the anisotropic state parameters and M_c is the critical state stress ratio.

3.6 Three-dimensional realization of the model

The MPZ model adopts the traditional $g(\theta)$ method for three-dimensional realization, and singularity often appears when this method is used in the numerical computation. YAO et al [21] pointed out that the three-dimensional yield surface of the model obtained by the $g(\theta)$ method is concave or discontinuous in some stress states, which will incur robustness insufficiency in the numerical computation. In addition, the shape of the yield surface on the π plane of the three-dimensional model with the $g(\theta)$ method doesn't vary with p. Moreover, many test results show that the strength envelope on the π plane tends to evolve from a curved triangle to a circle as p grows. Therefore, the modified stress mentioned above is converted into the transformed stress to reflect the effect of different Lode angles θ on the characteristics of yields on the π plane.

The modified stress $\bar{\sigma}_{ij}$ and the corresponding transformed stress $\tilde{\sigma}_{ij}$ are coaxial, and the mapping relation is expressed as follows:

$$\begin{cases} \tilde{\sigma}_{ij} = \bar{\sigma}_{ij}, \bar{q} = 0 \\ \tilde{\sigma}_{ij} = \bar{p}\delta_{ij} + \dfrac{\bar{q}_c}{\bar{q}}\left(\bar{\sigma}_{ij} - \bar{p}\delta_{ij}\right), \ \bar{q} \neq 0 \end{cases} \tag{56}$$

where $\bar{\sigma}_{ij}$ is the stress after the modification of the fabric tensor, i.e., the modified stress; $\tilde{\sigma}_{ij}$ is the stress after the transformation, namely the transformation stress; $\bar{q}_c$ refers to the deviatoric stress under the triaxial compression, which can be derived from the SMP strength criterion [35]:

$$\bar{q}_c = \frac{2\bar{I}_1}{3\sqrt{\left(\bar{I}_1\bar{I}_2 - \bar{I}_3\right)/\left(\bar{I}_1\bar{I}_2 - 9\bar{I}_3\right)} - 1} \tag{57}$$

where $\bar{I}_1$, $\bar{I}_2$, and $\bar{I}_3$ are respectively the three principal stress invariants corresponding to the modified stress.

3.7 Elastic stress−strain relationship

The stress−strain relationship of the elastic part adopts the generalized Hooke's law in the incremental form:

$$\mathrm{d}\varepsilon_{ij}^e = \frac{1+v}{E}\mathrm{d}\sigma_{ij} - \frac{3v}{E}\mathrm{d}p\delta_{ij} \tag{58}$$

where v is the Poisson ratio; $\mathrm{d}\sigma_{ij}$ is the stress tensor increment; δ_{ij} is the Kronecker tensor; and E is the modulus of elasticity, which can be expressed as:

$$E = \frac{3(1-2v)\left(1+e_0\right)}{\kappa}\left(p + p_s\right) \tag{59}$$

4 Laboratory tests and constants

To verify the rationality and effectiveness of the PZR model, a series of triaxial tests with different inclination angles for rockfills are chosen to simulate. The test material is the main rockfills of the Rumei high core rockfill dam. The large-scale static and dynamic true triaxial apparatus of Tsinghua University is used [44], which adopts a mixed loading form, and can apply the maximum confining pressure of 20 MPa. The maximum size of the specimen is 20 cm×20 cm×40 cm and the maximum grain size is 40 mm. The specimens of the inclined compaction plane are prepared by the special mould [10], and the direction of the compaction plane is shown in Figure 5. Table 1 summaries the scheme of the triaxial compression tests.

There are 17 constants in the PZR model, in which κ and v are elastic constants; λ, N and Z are constants of the crushing stress; α_f and M_{fc} are the constants of loading direction; m_g, m and M_{gc} are constants of dilatancy equation; H_0, H_{U0}, m_b and β_H are constants of plastic modulus; Δ, r and Γ are anisotropic constants. All constants can be obtained by triaxial tests. Among these constants, the anisotropic constants can be obtained by fitting the conventional triaxial tests with different direction angles. The model constants of Rumei rockfills are shown in Table 2.

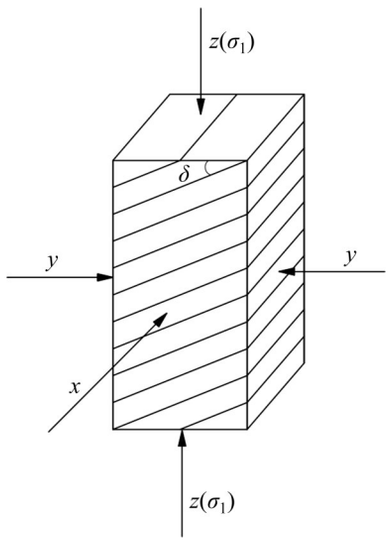

Figure 5 Diagram illustrating direction of compaction plane

Table 1 Test scheme and stress path

Type	Stress path	Dry density, ρ_d/(g·cm^{-3})
Triaxial tests with different inclination angles	δ=0°, 15°, 30°, 45°, 60°, 75°, 90° in σ_3=400 kPa; δ=0°, 15°, 45°, 75°, 90° in σ_3=800 kPa; δ=0° in σ_3=200 kPa and 1200 kPa; load to ε_1=15%	2.05

Table 2 PZR model constants of Rumei dam main rockfill

κ	ν	λ	N	Z	α_f
0.015	0.1	0.125	1.38	0.55	0.25
M_{fc}	M_{gc}	H_0	H_{U0}	m_g	m_b
1.5	1.9	600	1000	0.8	0.175
m	β_H	Δ	r	Γ	
1	2	0.316	4.2	0.25	

5 Verification of constitutive model

5.1 Simulation of conventional triaxial compression tests with different confining pressures

The test results of a group of conventional triaxial compression tests with δ=0° and the simulation results of the PZR model are plotted in the same figure, as shown in Figure 6. Figure 6(a) illustrates the relationships between the deviatoric stress and the axial strain under different confining pressures, which demonstrate the capacity of the PZR model to well reflect the nonlinearity and

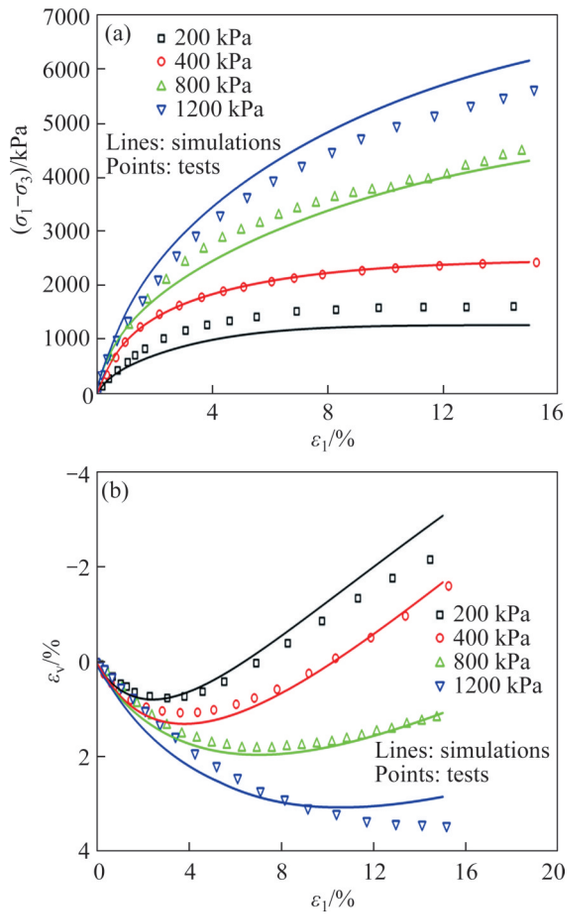

Figure 6 Simulation of conventional triaxial compression test results with PZR model: (a) $(\sigma_1-\sigma_3)-\varepsilon_1$ relationships; (b) $\varepsilon_v-\varepsilon_1$ relationships

compressive hardening of the rockfill. Figure 6(b) presents the relationships between the volumetric strain and the axial strain under different confining pressures. With the increase of confining pressure, the dilatancy of rockfill decreases gradually, which verify the ability of the PZR model to well reflect the volumetric deformation characteristics of the rockfill materials.

5.2 Simulation of triaxial compression tests with different inclination angles of compaction plane

Figure 7 compares the simulation results of triaxial tests with 7 different δ values under a confining pressure of 400 kPa with the test data. As shown in Figure 7(a), the model can reflect the significant difference in the mechanical properties caused by the initial anisotropy resulting from the directional arrangement of grains. The simulation results and the test results are basically consistent

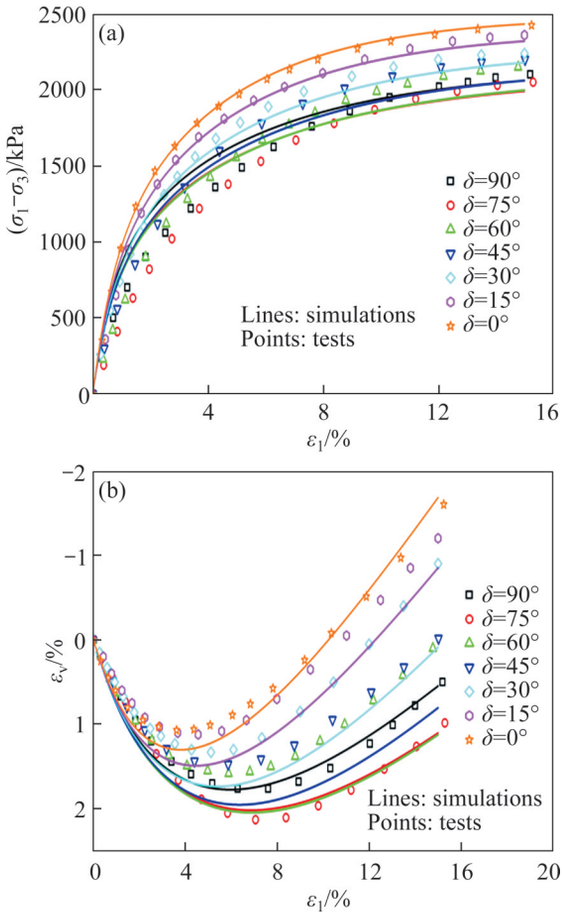

Figure 7 Conventional triaxial test results and simulation results of different inclination angles of compaction plane under a confining pressure of 400 kPa: (a) $(\sigma_1-\sigma_3)-\varepsilon_1$ relationships; (b) $\varepsilon_v-\varepsilon_1$ relationships

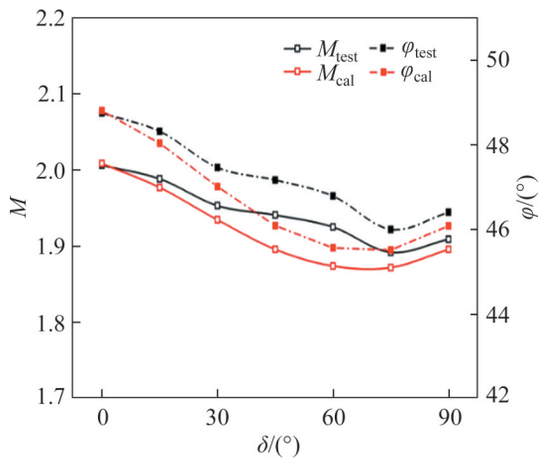

Figure 8 Comparison of simulation strengths and test results of triaxial drained shear tests with different inclination angles of compaction plane under a confining pressure of 400 kPa

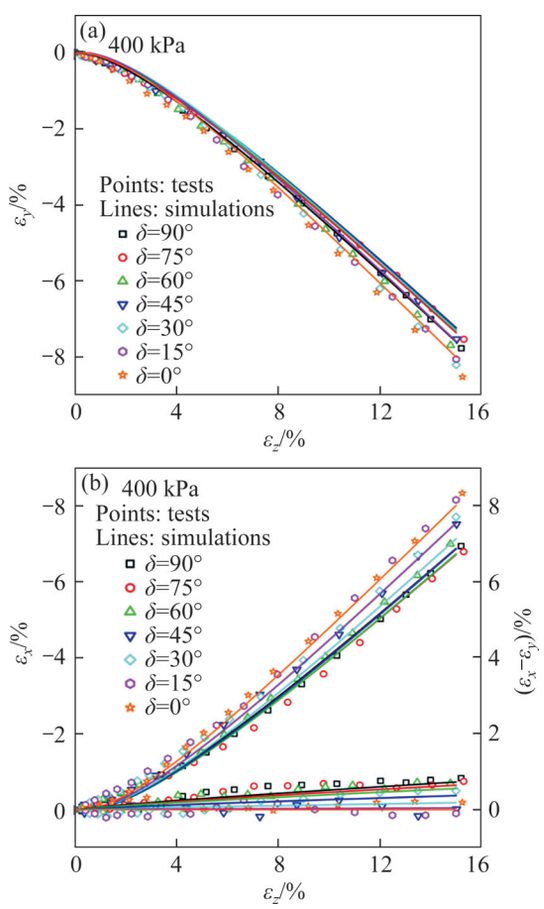

Figure 9 Lateral strain results of conventional triaxial tests with different inclination angles of compaction plane and corresponding simulation results under a confining pressure of 400 kPa: (a) $\varepsilon_y-\varepsilon_z$ relationships; (b) $\varepsilon_x-\varepsilon_z$ and $(\varepsilon_x-\varepsilon_y)-\varepsilon_z$ relationships

when ε_1=15%. According to Figure 7(b), the simulation results and the test results share good consistency when δ equals 0°, 75° and 90°, while they differ from each other to a certain extent when δ falls in the other interval, but the overall trends match well.

Figure 8 shows a comparison of strength simulation and test results of conventional triaxial compression tests with different inclination angles. It can be seen that the model can effectively reflect the basic change characteristic and magnitude of the peak stress ratio M and peak internal friction angle φ caused by the change of δ value.

Figure 9 shows the test results of lateral strain of triaxial test with different inclination angles and corresponding PZR model simulation results under confining pressure of 400 kPa. The lateral normal strains ε_y and ε_x present the maximum lateral expansion deformation at δ=0°, which is related to the maximum volumetric dilatation of the specimen at δ=0°. Moreover, lateral strains in the

two directions are the most similar when $\delta=0°$, which is consistent with the cognition on the equal lateral deformation in the transversely isotropic soil. As shown in Figure 9(b), according to the simulation results of the PZR model, the difference between the two lateral normal strains increases as δ grows, and the amount of expansion in the direction of ε_y is greater than that in the direction of ε_x. These characteristics of lateral deformation are well captured by the PZR model.

The simulation results and the test data of the triaxial tests with different δ values under a confining pressure of 800 kPa are plotted in Figure 10. As shown in Figure 10(a), stress−strain curves corresponding to different δ values are more similar when the confining pressure is higher, which has been captured by the PZR model. This phenomenon is speculated to result from the stronger constraint of a higher confining pressure on the anisotropy. Moreover, the grain crushing also increases as the confining pressures rises. As shown in Figure 10(b), for different δ values, the simulation volumetric variation is in good agreement with the test results on the whole.

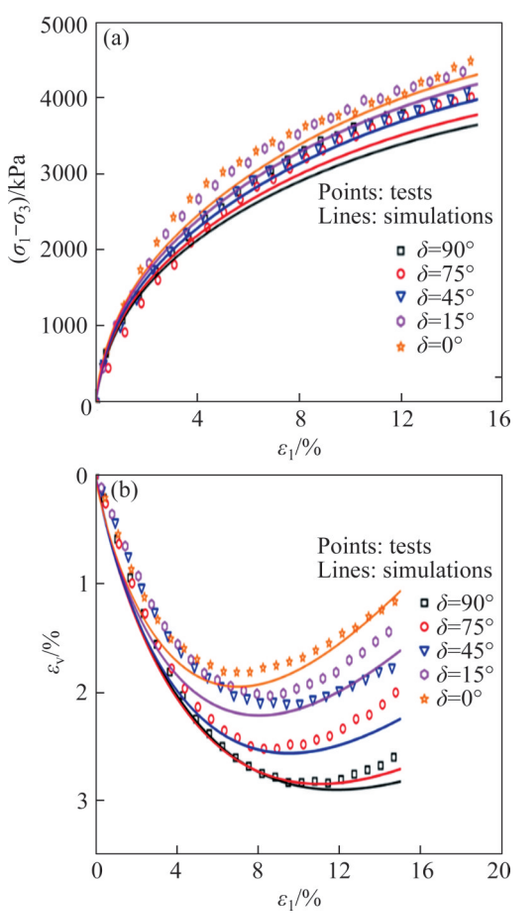

Figure 10 Conventional triaxial test results and simulation results of different inclination angles of compaction plane under a confining pressure of 800 kPa: (a) $(\sigma_1-\sigma_3)-\varepsilon_1$ relationships; (b) $\varepsilon_v-\varepsilon_1$ relationships

6 Conclusions

In this study, an improved generalized plasticity model for rockfill materials (PZR model) is developed from the MPZ model based on a new anisotropic state parameter. The PZR model takes into consideration of the anisotropy and grain crushing of rockfill materials in the practical engineering. Then this model is used to simulate a series of test results of the main rockfill materials of the Rumei high core rockfill dam, followed by a detailed analysis.

1) Different relative relationships between the grain arrangement direction and the dominant shear direction lead to different state parameters, thereby resulting in different influences on the development of stress and deformation of rockfill materials. Considering this mechanism, the anisotropy state index ω is constructed according to the angle (α_{min}) between the SMP and the compaction plane. Using the modified stress method to describe the anisotropic fabric can comprehensively consider the influence of the true three-dimensional stress state on the real strain values in all directions. The anisotropic state index can make up for the shortcoming that the modified stress method cannot reflect the non-monotonic variation of the peak strength of anisotropy as the inclination angle of the compaction plane varies.

2) The contribution of work done by p and q to grain crushing is considered respectively by the crushing stress p_s with clear physical meaning and the offset of ACL caused by shear. According to the anisotropic state index ω, the state parameter ξ is defined. Instead of calculating the state parameter by the fixed critical state line, this study elaborates the influences of anisotropy and grain crushing on the relative spatial position of the reference state line. Therefore, the main characteristics of stress and deformation of rockfill materials in practice can be reflected theoretically. Based on these relations, an improved generalized plasticity model for rockfill materials (PZR model) is established, which adopts the modified dilatancy equation and the

transformation stress method.

3) The stress−strain relationship simulated by the PZR model for conventional triaxial compression tests is in good agreement with the test results, which indicates that the PZR model can reflect the basic characteristics of stress and deformation of rockfill materials under different confining pressures when considering grain crushing.

4) The simulation results of the PZR model for two groups of conventional triaxial compression tests with different inclination angles are in good agreement with the test results, which indicates the capacity of the PZR model to reflect the obvious difference of mechanical properties caused by the initial anisotropy of rockfill materials. The reason is that the variation trend of the anisotropy index ω can reflect the non-monotonic variation of the deformation and the strength of rockfill materials as the inclination angle δ varies. At the same time, due to the introduction of the modified stress tensor, the model can simulate the lateral deformation difference caused by the inclination of compaction plane. The simulation results show that the PZR model has a good description of the anisotropy and grain crushing characteristics of rockfill materials.

Contributors

The overarching research goals were developed by WANG Xiang-nan and YU Yu-zhen. ZHAN Zheng-gang provided the study cases. ZHANG Xiang-tao, GAO Yi-zhao and WANG Xiang-nan established the models, completed the program construction and calculated the study cases. The initial draft of the manuscript was written by WANG Xiang-nan, GAO Yi-zhao, ZHANG Xiang-tao. ZHANG Xiang-tao, GAO Yi-zhao, WANG Xiang-nan, YU Yu-zhen replied to reviewers' comments and revised the final version.

Conflict of interest

ZHANG Xiang-tao, GAO Yi-zhao, WANG Xiang-nan, YU Yu-zhen, ZHAN Zheng-gang declare that they have no conflict of interest.

Reference

[1] ZHAO Chong-bin. Physical and chemical dissolution front instability in porous media: Theoretical analyses and computational simulations [M]. Berlin: Springer, 2014: 354. https://link.springer.com/book/10.1007%2F978-3-319-08461-9.

[2] ZHAO Chong-bin. Dynamic and transient infinite elements: Theory and geophysical, geotechnical and geoenvironmental applications [M]. Berlin: Springer, 2009: 259. https://www.springer.com/gp/book/9783642008450.

[3] ZHAO Chong-bin, HOBBS B E, ORD A. Fundamentals of computational geoscience: Numerical methods and algorithms [M]. Berlin: Springer, 2009: 285. http://www.gbv.de/dms/goettingen/584426224.pdf.

[4] SYMES M J P R, GENS A, HIGHT D W. Undrained anisotropy and principal stress rotation in saturated sand [J]. Géotechnique, 1984, 34(1): 11−27. DOI: 10.1680/geot.1984.34.1.11.

[5] ABELEV A V, LADE P V. Effects of cross anisotropy on three-dimensional behavior of sand. I: Stress−strain behavior and shear banding [J]. Journal of Engineering Mechanics, 2003, 129(2): 160 − 166. DOI: 10.1061/(asce)0733-9399(2003)129: 2(160).

[6] GEORGIANNOU V N, KONSTADINOU M, TRIANTAFYLLOS P. Sand behavior under stress states involving principal stress rotation [J]. Journal of Geotechnical and Geoenvironmental Engineering, 2018, 144(6): 04018028. DOI: 10.1061/(asce)gt.1943-5606.0001878.

[7] ZAMANIAN M, MOLLAEI-ALAMOUTI V, PAYAN M. Directional strength and stiffness characteristics of inherently anisotropic sand: The influence of deposition inclination [J]. Soil Dynamics and Earthquake Engineering, 2020, 137: 106304. DOI: 10.1016/j.soildyn.2020.106304.

[8] ARTHUR J R F, MENZIES B K. Inherent anisotropy in a sand [J]. Géotechnique, 1972, 22(1): 115−128. DOI: 10.1680/geot.1972.22.1.115.

[9] ODA M, KOISHIKAWA I, HIGUCHI T. Experimental study of anisotropic shear strength of sand by plane strain test [J]. Soils and Foundations, 1978, 18(1): 25 − 38. DOI: 10.3208/sandf1972.18.25.

[10] ZHANG Xiang-tao, GAO Yi-zhao, WANG Yuan, et al. Experimental study on compaction-induced anisotropic mechanical property of rockfill material [J]. Frontiers of Structural and Civil Engineering, 2021, 15(1): 109 − 123. DOI: 10.1007/s11709-021-0693-0.

[11] MARSAL R J. Large scale testing of rockfill materials [J]. Journal of the Soil Mechanics and Foundations Division, 1967, 93(2): 27−43. DOI: 10.1061/jsfeaq.0000958.

[12] XIAO Yang, LIU Han-long, DING Xuan-ming, et al. Influence of particle breakage on critical state line of rockfill material [J]. International Journal of Geomechanics, 2016, 16(1): 04015031. DOI: 10.1061/(asce)gm.1943-5622.0000538.

[13] LIU Meng-cheng, GAO Yu-feng, LIU Han-long. An elastoplastic constitutive model for rockfills incorporating energy dissipation of nonlinear friction and particle breakage [J]. International Journal for Numerical and Analytical Methods in Geomechanics, 2014, 38(9): 935 − 960. DOI: 10.1002/nag.2243.

[14] HARDIN B O. Crushing of soil particles [J]. Journal of Geotechnical Engineering, 1985, 111(10): 1177−1192. DOI:

10.1061/(asce)0733-9410(1985)111: 10(1177).

[15] ZIENKIEWICZ O C, MROZ Z. Generalized plasticity formulation and applications to geomechanics [C]// DESAI C S, GALAGHER R H. Mechanics of Engineering Materials. Chichester: Wiley, 1984: 655 − 679. https://www.researchgate.net/publication/284254804.

[16] PASTOR M, ZIENKIEWICZ O C, CHAN A H C. Generalized plasticity and the modelling of soil behaviour [J]. International Journal for Numerical and Analytical Methods in Geomechanics, 1990, 14(3): 151 − 190. DOI: 10.1002/nag.1610140302.

[17] KHOEI A R, AZAMI A R, HAERI S M. Implementation of plasticity based models in dynamic analysis of earth and rockfill dams: A comparison of Pastor-Zienkiewicz and cap models [J]. Computers and Geotechnics, 2004, 31(5): 384 − 409. DOI: 10.1016/j.compgeo.2004.04.003.

[18] XU Bin, ZOU De-gao, KONG Xian-jing, et al. Dynamic Damage evaluation on the slabs of the concrete faced rockfill dam with the plastic-damage model [J]. Computers and Geotechnics, 2015, 65: 258 − 265. DOI: 10.1016/j. compgeo. 2015.01.003.

[19] LIU Meng-cheng, GAO Yu-feng. Constitutive modeling of coarse-grained materials incorporating the effect of particle breakage on critical state behavior in a framework of generalized plasticity [J]. International Journal of Geomechanics, 2017, 17(5): 04016113. DOI: 10.1061/(asce)gm.1943-5622.0000759.

[20] DONG Wei-xin. Fluid-solid coupling elastoplastic seismic dynamic response analysis of high core rockfill dam [D]. Beijing: Tsinghua University, 2015. http://cdmd.cnki.com.cn/Article/CDMD-10003-1016712265.htm. (in Chinese)

[21] YAO Yang-ping, WANG Nai-dong. Transformed stress method for generalizing soil constitutive models [J]. Journal of Engineering Mechanics, 2014, 140(3): 614 − 629. DOI: 10.1061/(asce)em.1943-7889.0000685.

[22] TIAN Yu, YAO Yang-ping. A simple method to describe three-dimensional anisotropic failure of soils [J]. Computers and Geotechnics, 2017, 92: 210 − 219. DOI: 10.1016/j.compgeo.2017.08.004.

[23] LIU Si-hong, SHAO Dong-chen, SHEN Chao-min, et al. Microstructure-based elastoplastic constitutive model for coarse-grained materials [J]. Chinese Journal of Geotechnical Engineering, 2017, 39(5): 777−783.

[24] HARDIN B O, RICHART F E. Elastic wave velocities in granular soils [J]. Journal of the Soil Mechanics and Foundations Division, 1963, 89(1): 33 − 65. DOI: 10.1061/jsfeaq.0000493.

[25] ROSCOE K H, SCHOFIELD A N, WROTH C P. On the yielding of soils [J]. Géotechnique, 1958, 8(1): 22 − 53. DOI: 10.1680/geot.1958.8.1.22.

[26] LI X S, DAFALIAS Y F. Dilatancy for cohesionless soils [J]. Géotechnique, 2000, 50(4): 449 − 460. DOI: 10.1680/geot.2000.50.4.449.

[27] BEEN K, JEFFERIES M G. A state parameter for sands [J]. Géotechnique, 1985, 35(2): 99 − 112. DOI: 10.1680/geot.1985.35.2.99.

[28] LI X S, DAFALIAS Y F. Dilatancy for cohesionless soils [J]. Géotechnique, 2000, 50(4): 449 − 460. DOI: 10.1680/geot.2000.50.4.449.

[29] LING H I, YANG Song-tao. Unified sand model based on the critical state and generalized plasticity [J]. Journal of Engineering Mechanics, 2006, 132(12): 1380 − 1391. DOI: 10.1061/(asce)0733-9399(2006)132: 12(1380).

[30] MANZANAL D, PASTOR M, MERODO J A F. Generalized plasticity state parameter-based model for saturated and unsaturated soils. Part II: Unsaturated soil modeling [J]. International Journal for Numerical and Analytical Methods in Geomechanics, 2011, 35(18): 1899 − 1917. DOI: 10.1002/nag.983.

[31] AKHAVEISSY A H. Analysis of tunnel and super structures for excavation [J]. Scientia Iranica, 2011, 18(1): 1 − 8. DOI: 10.1016/j.scient.2011.03.001.

[32] WONG R K S, ARTHUR J R F. Induced and inherent anisotropy in sand [J]. Géotechnique, 1985, 35(4): 471−481. DOI: 10.1680/geot.1985.35.4.471.

[33] ODA M, NAKAYAMA H. Introduction of inherent anisotropy of soils in the yield function [M]// Studies in Applied Mechanics. Amsterdam: Elsevier, 1988: 81 − 90. DOI: 10.1016/b978-0-444-70523-5.50017-5.

[34] TOBITA Y. Fabric tensors in constitutive equations for granular materials [J]. Soils and Foundations, 1989, 29(4): 91−104. DOI: 10.3208/sandf1972.29.4_91.

[35] MATSUOKA H, NAKAI T R. Stress-deformation and strength characteristics of soil under three different principal stresses [J]. Proceedings of the Japan Society of Civil Engineers, 1974, 1974(232): 59 − 70. DOI: 10.2208/jscej1969.1974.232_59.

[36] WANG Yuan, ZHANG Sheng, AO Da-hua, et al. Particle breakage characteristics of rockfills under complex stress paths [J]. Chinese Journal of Geotechnical Engineering, 2018, 40(4): 698−706.

[37] LUO Ting, LIU Lin, YAO Yang-ping. Description of critical state for sands considering particle crushing [J]. Chinese Journal of Geotechnical Engineering, 2017, 39(4): 592−600.

[38] YAO Yang-ping, LIU Lin, LUO Ting, et al. Unified hardening (UH) model for clays and sands [J]. Computers and Geotechnics, 2019, 110: 326 − 343. DOI: 10.1016/j.compgeo.2019.02.024.

[39] PESTANA J M, WHITTLE A J. Compression model for cohesionless soils [J]. Géotechnique, 1995, 45(4): 611 − 631. DOI: 10.1680/geot.1995.45.4.611.

[40] SHEN Chao-min, LIU Si-hong, WANG Liu-jiang, et al. Micromechanical modeling of particle breakage of granular materials in the framework of thermomechanics [J]. Acta Geotechnica, 2019, 14(4): 939 − 954. DOI: 10.1007/s11440-018-0692-z.

[41] NOVA R, WOOD D M. A constitutive model for sand in triaxial compression [J]. International Journal for Numerical and Analytical Methods in Geomechanics, 1979, 3(3): 255 − 278. DOI: 10.1002/nag.1610030305.

[42] ROSCO K H, BURLAND J B. On generalized stress strain behavior of wet clay [J]. Engineering Plasticity, 1968, 535 − 609. https://www.researchgate.net/publication/26492 1746.

[43] FU Zhong-zhi, CHEN Sheng-shui, SHI Bei-xiao. Large-scale triaxial experiments on the creep behavior of a saturated rockfill material [J]. Journal of Geotechnical and Geoenvironmental Engineering, 2018, 144(7): 04018039. DOI: 10.1061/(asce)gt.1943-5606.0001898.

[44] WANG Yuan, YU Yu-zhen, WU Yong-kang, et al. Development and application of a large-scale static and dynamic true triaxial apparatus for gravel [J]. International Journal of Geomechanics, 2018, 18(3): 04018004. DOI: 10.1061/(asce)gm.1943-5622.0001096.

(Edited by HE Yun-bin)

中文导读

考虑颗粒破碎与各向异性的堆石料广义塑型模型

摘要：堆石料以其填筑密度高、压实性能好、透水性强、沉降变形小、承载力高等优点，在堆石坝、铁路、公路路基等工程建设中得到广泛应用。合理的堆石料本构模型对工程计算和分析具有重要意义，且目前仍具有很大的发展空间。基于破碎应力和空间滑动面(SMP)的概念，提出了一个能综合反映颗粒破碎和各向异性的状态参数。利用该状态参数对修正ZienkiewiczIII模型(MPZ模型)进行了改进，构造了一个能够描述堆石料应力变形工程特性的广义塑性模型。本文通过一系列不同压实面倾角的常规三轴试验，验证了该模型的有效性。由于所构造的各向异性指标ω的变化趋势能够反映堆石料的变形和强度随大主应力方向角非单调变化的特征，故该模型可以反映堆石料初始各向异性对力学特性造成的明显差异。

关键词：本构模型；各向异性；颗粒破碎；堆石料